Electrical Power and Energy Systems 131 (2021) 107006

Contents lists available at ScienceDirect

International Journal of Electrical Power and Energy Systems

journal homepage: www.elsevier.com/locate/ijepes

On WAMS-based emergency outage detection using optimization

Stefan Polster [*,1], Herwig Renner, Robert Schürhuber, Katrin Friedl

Institute of Electrical Power Systems – Graz University of Technology, Austria

ARTICLE INFO

Keywords:
Outage detection
Hybrid optimizer
PMU
Particle swarm optimization
Power transmission systems

ABSTRACT

In this paper, an optimization-based algorithm for the detection of multi-branch outages is presented. The main advantage is its ability to detect an unknown number of tripped branches in meshed power systems solely based on node voltage angle information obtained with phasor measurement units (PMUs). The proposed algorithm uses a hybrid optimization approach combining particle swarm optimization with Newton's method. The algorithm is tested on linearized load flow data as well as on a dynamic simulation of the Nordic-32-Bus system. In a sensitivity analysis the influence of the optimizer's main parameters and the robustness against linearization errors and missing data is shown. The high ratio of correct detection results across the whole range of evaluated parameters identifies the proposed algorithm as a useful supportive tool for future decentralized SCADA applications.

1. Introduction

Accurate state awareness of a system is an important factor for secure grid operation. The system state is usually provided by state estimators. Traditionally, the input data of state estimators consists of the topology and asynchronous measurements – voltage, current, power, etc. – based on SCADA systems with update rates down to several seconds. With the increasing exploitation of PMUs, algorithms for dynamic state estimators are being developed using the synchronized and quickly updated measurements [1–3] available now. However, the correct system topology remains a crucial factor in the quality of the state estimation. Therefore, an accurate detection of branch outages is of great importance. A special problem situation arises in grid areas on the responsibility border of different grid operators, where only sparse real time information is shared. Recent work on outage detection focuses on a joint detection and estimation problem [4] to accurately update state estimator's topology model using all kind of available measurements from unsynchronised power, voltage and current magnitudes as well as synchronised voltage phasor measurements.

Several publications of the last years focused on the problem of outage detection using synchro phasor data and evaluated a wide range of possible algorithms. The following review is far from complete but shall give an overview on already evaluated approaches.

In [5] a method is described using pre simulated linearized node voltage angle sensitivities on branch outages to detect a tripped branch. Later this method is developed further to be used for double branch outages [6] and applied on specific parts of large networks to reduce the necessary synchro phasor data [7]. Similar to these works, a detection algorithm based on the least square error between measured and simulated node voltage angles is discussed and evaluated on its vulnerability to bad WAMS data [8] and another detection estimation algorithm is proposed using bus power mismatches calculated from node voltage angles decision criterion [9]. However, all of these approaches need the number of tripped branches as input and require the pre-calculation of the sensitivities after any change in the network topology. The necessary effort for these pre-calculations increase with the number of considered branches and has to be repeated after any change in the network.

The use of a decision tree identifying critical attributes in WAMS data and further applying them as detection criterion is discussed in [10]. The contingencies detectable with this approach are not limited to branch outages, but it comes at the cost of extensive pre-simulations since any considered contingencies has to be simulated and the decision tree trained on the set of contingencies.

Another method as described in [11] is based on vector estimation which is solved with adopted greedy orthogonal matching pursuit as well as the convex least-absolute shrinkage and selection operator. This method can overcome the need of a beforehand known number of tripped branches by incorporating an additional sample variance deviation criterion based on pre-calculations but requires information on line outage probabilities and expected noise level.

* Corresponding author.
E-mail address: stefan.polster@tugraz.at (S. Polster).
[1] Recipient of a DOC Fellowship of the Austrian Academy of Sciences at the Institute of Electrical Power Systems, TU Graz, Austria.

https://doi.org/10.1016/j.ijepes.2021.107006
Received 9 October 2020; Received in revised form 12 February 2021; Accepted 9 March 2021
Available online 30 April 2021

Nomenclatures

List of Symbols

HPN	**H**ybrid **P**article Swarm – **N**ewton Optimizer
HVDC	**H**igh **V**oltage **D**irect **C**urrent
PSO	**P**article **S**warm **O**ptimizer
PMU	**P**hasor **M**easurement **U**nit
VSC	**V**oltage **S**ource **C**onverter
WAMS	**W**ide **A**rea **M**easurement **S**ystem
$\boldsymbol{\delta}$	Newton step
ε	optimality tolerance
$\boldsymbol{\vartheta}$	node voltage angle, referred to slack node, dimension $(N-1)\times 1$
$\Delta\boldsymbol{\vartheta}$	calculated change in node voltage angle after contingency event, dimension $(N-1)\times 1$
$\Delta\boldsymbol{\vartheta}_{\text{meas}}$	measured change in node voltage angle after contingency event, dimension $(N_{\text{PMU}}-1)\times 1$
ξ	detection threshold
$\mathbf{A}_{\text{PMU}}$	PMU incidence matrix, dimension $N_{\text{PMU}}\times(N-1)$
$\mathbf{A}_{\text{LOI}}$	branch of interest incidence matrix, dimension $L\times L_{\text{OI}}$
$\mathbf{B}$	node susceptance matrix, dimension $(N-1)\times(N-1)$
b	index denoting pre-contingency situation
c	index denoting post-contingency situation
c_1, c_2	weighting factors of the updating formula used in the PSO
f	objective function
$\boldsymbol{\Delta} f$	gradient of objective function
$\mathbf{H}$	Hessian of objective function
i	iteration step
$i_{\max}$	maximum iteration step
j	one specific particle of the PSO
$\mathbf{K}_{\text{D}}$	full correlation matrix between $\Delta\mathbf{p}_{\text{NL}}$ and $\Delta\boldsymbol{\vartheta}$
$\mathbf{K}_{x_B}$	according to $\mathbf{x}_{\text{B}}$ reduced correlation matrix between $\mathbf{x}_{\text{p}}$ and $\Delta\boldsymbol{\vartheta}$
L	number of branches in the network
ℓ	notation of a specific branch
L_{OI}	number of branches of interest
N	number of nodes in the network including slack node
n	notation of a specific node
N_{PMU}	number of PMU monitored nodes
$\mathbf{NBI}$	node-to-branch incidence matrix, dimension $(N-1)\times L$
$\mathbf{p}_{\text{p}}$	particle's personal best position in PSO
$\mathbf{p}_{\text{g}}$	global best position in PSO
$\mathbf{p}_{\text{N}}$	node power injections, dimension, $(N-1)\times 1$
$\Delta\mathbf{p}_{\text{N}}$	fictional change in node power injections modelling the effects of a contingency event, dimension $(N-1)\times 1$
$\Delta\mathbf{p}_{\text{NL}}$	fictional change in node power injections referred to branches, dimension $L\times 1$
r_1, r_2	equally distributed random numbers of the updating formula used in the PSO
$\mathbf{v}_{\text{B}}$	particle velocity used in PSO
w	particle's inertia factor of the updating formula used in the PSO
$\mathbf{x}_{\text{B}}$	trial variable linked to branches
$\mathbf{x}_{\text{P}}$	trial variable linked to node power injection

The exploitation of statistical properties of the generation and demand of the considered network in combination with an application of quickest change detection algorithm on node voltage angle measurements to detect transmission line outages is discussed in [12] and further evaluated in [13,14]. Based on this approach the ideal location of measurements and possible improvements by system partitioning are evaluated in [15]. This method is applicable on single and multi-branch outages, but due its need to parallelly applying the Cumulative Sum algorithm for each possible outage combination the computational burden is rather high. A comparison on statistical based outage detection is given in [16].

Several papers use optimisation-based approaches. For examples the work described in [17] utilizes mixed-integer programming to identify line outages in an external system influencing load flow of the internal system. This approach is only applied on single branch outages. An evolutionary optimisation-based approach is using an adaptive version of distribution algorithm [18]. This algorithm seems to be able to detect a variable number of tripped branches and is further developed in [19]. However, from the results it is unclear, if it is suitable for a fast detection in real operation conditions.

In contrast to these works, the goal of the proposed algorithm is to provide an accurate detection of tripped branches based on minimal information which can be used for decentralized emergency control decisions – e.g., to automatically activate a superordinate controller of HVDC links as used in [20] and [21]. Therefore, the computational complexity of the algorithms should be not too demanding, so as to enable decent runtimes for a near to real time detection. Additionally, the algorithm's performance must be independent from the pre-contingency load flow. These postulations encourage the use of linearized cold start models, such as the classical DC load flow [22], for the problem formulation and WAMS measured changes of the node voltage angles caused by the tripped branches.

The algorithm evaluated in this paper focuses on the use of optimizers to solve the detection problem, whereby a hybrid optimizer combining particle swarm optimization with Newton's method henceforth referred to as HPN (**H**ybrid **P**article Swarm – **N**ewton Optimizer), is implemented. The HPN was selected due to pre-evaluations comparing its performance to an adapted Newton's method and particle swarm optimization.

This paper is subsequently organized as follows: Section 2 is dedicated to the definition of the optimizer's objective function. The implemented algorithm is described in Section 3. The simulated network and simulations are given in Section 4 and the detection results based on the simulation data are discussed in Section 5. Finally, the conclusions are stated in Section 6.

2. Definition of the objective function for optimisation

The objective function is defined as the mean square error between the PMU measured voltage angle changes and the estimated voltage angle changes. The estimated voltage angle changes are a function of the trial variable of the optimization based on the linearized DC load flow network model. For the following, an arbitrary network with N nodes and L branches is assumed. Due to the linearization, the node voltage angles $\boldsymbol{\vartheta}$ are calculated solely as a function of the active node power injections $\mathbf{p}_{\text{N}}$ and the node susceptance matrix $\mathbf{B}$

$$\boldsymbol{\vartheta} = \mathbf{B}^{-1}\cdot\mathbf{p}_{\text{N}} \tag{2-1}$$

$$\boldsymbol{\vartheta}\in\mathbb{R}^{(N-1)\times 1},\ \mathbf{p}_{\text{N}}\in\mathbb{R}^{(N-1)\times 1},\ \mathbf{B}\in\mathbb{R}^{(N-1)\times(N-1)} \tag{2-2}$$

Any change in the active node power injections leads to a change in the node voltage angles. Furthermore, any branch outage which does not isolate a part of the network can be represented by a fictional power injection at the starting node and an equally high negative power injection at the branch's ending node [23]. The fictional power injections' value is defined by the condition, that the resulting branch load of the tripped branch has to be 0. The change of the node voltage angles $\Delta\boldsymbol{\vartheta}$ is therefore calculated with the fictional power injection vector $\Delta\mathbf{p}_{\text{N}}$ and the unchanged node susceptance matrix. The resulting change of the node voltage angles corresponds to the effects of a branch outage, if $\Delta\mathbf{p}_{\text{N}}$

is composed of the fictional power injections modelling a branch outage.

$$\Delta\boldsymbol{\vartheta} = \mathbf{B}^{-1}\cdot\Delta\mathbf{p}_{\mathrm{N}} = \mathbf{B}^{-1}\cdot\mathbf{NBI}\cdot\Delta\mathbf{p}_{\mathrm{NL}} \tag{2-3}$$

$$\begin{aligned}\Delta\boldsymbol{\vartheta} &\in \mathbb{R}^{(N-1)\times 1}\\ \Delta\mathbf{p}_{\mathrm{NL}} &\in \mathbb{R}^{L\times 1}\\ \mathbf{NBI} &\in \{-1,0,1\}^{(N-1)\times L}\end{aligned} \tag{2-4}$$

The usage of the node-to-branch incidence matrix **NBI** and a vector $\Delta\mathbf{p}_{\mathrm{NL}}$ containing one value of a fictional power injection for each branch in the network allows a direct linking of multi branch outages to the node voltage angle change. The elements of $\Delta\mathbf{p}_{\mathrm{NL}}$ are 0 except for those corresponding to the branches tripped. $\Delta\mathbf{p}_{\mathrm{NL}}$ can easily be calculated if the tripped branches and the change of the node voltage angles are known.

However, since the branches tripped and their number are unknown, a suitable solution for $\Delta\mathbf{p}_{\mathrm{NL}}$ is found by minimizing the mean square error function between the measured and calculated node voltage angle change. The scalar objective function in respect to the trial variable $\Delta\mathbf{p}_{\mathrm{NL}}$ is stated as

$$f(\Delta\mathbf{p}_{\mathrm{NL}}) = \left\|\Delta\boldsymbol{\vartheta}_{\mathrm{meas}} - \mathbf{K}_{\mathrm{D}}\cdot\Delta\mathbf{p}_{\mathrm{NL}}\right\|^2 \tag{2-5}$$

$$\mathbf{K}_{\mathrm{D}} = \mathbf{B}^{-1}\cdot\mathbf{NBI} \tag{2-6}$$

$$\mathbf{K}_{\mathrm{D}} \in \mathbb{R}^{(N-1)\times L} \tag{2-7}$$

$\mathbf{K}_{\mathrm{D}}$ is a matrix describing the relation between node voltage angle change $\Delta\boldsymbol{\vartheta}$ and the trial variable $\Delta\mathbf{p}_{\mathrm{NL}}$. The slack node, defining the reference angle, is excluded. In general, not all branches of the network are of interest and not all nodes are equipped with a PMU. The number of branches of interest are denoted in the following as L_{OI} and the number of PMU monitored nodes as N_{PMU}. This leads to the necessity to define incidence matrices that relate PMU monitored nodes and branches of interest to the nodes and branches of the complete network. The PMU incidence matrix $\mathbf{A}_{\mathrm{PMU}}$ relates the nodes and the branch of interest incidence matrix $\mathbf{A}_{\mathrm{LOI}}$ the branches. The objective function changes to

$$f(\Delta\mathbf{p}_{\mathrm{NL}}) = \left\|\Delta\boldsymbol{\vartheta}_{\mathrm{meas}} - \mathbf{A}_{\mathrm{PMU}}\cdot\mathbf{K}_{\mathrm{D}}\cdot\mathbf{A}_{\mathrm{LOI}}\cdot\Delta\mathbf{p}_{\mathrm{NL}}\right\|^2 \tag{2-8}$$

$$\mathbf{A}_{\mathrm{PMU}} \in \{0,1\}^{N_{\mathrm{PMU}}\times(N-1)} \tag{2-9}$$

$$\mathbf{A}_{\mathrm{LOI}} \in \{0,1\}^{L\times L_{\mathrm{OI}}} \tag{2-10}$$

From Eq. (2-3), it is concluded that a minimum of the objective function must exist for a trial variable vector $\Delta\mathbf{p}_{\mathrm{NL}}$ only containing nonzero values at the elements corresponding to the branches actually tripped. The value of the objective function at this optimality point is 0. This is the case if the DC load flow solutions matches the measured data exactly, which, generally, is not the case. However, due to the relatively small expectable angle error of the DC load flow, it can be assumed that the optimization still finds a $\Delta\mathbf{p}_{\mathrm{NL}}$ vector with dominant values at the elements corresponding to the branches actually tripped.

The representation of double lines in the objective function prevents a distinguishable detection for parallel branches. Without a suitable pre-evaluation of the network topology, the results of the optimizer are not unambiguous, since the outage of one or more of the parallel branches will lead to an optimal trial variable $\Delta\mathbf{p}_{\mathrm{NL}}$. Only the values of the nonzero elements can give further information about the actual outage – higher values can be expected for multi branch outages. However, these values also depend on the pre-fault state of the system, thus making it necessary to include the load flow situation. The distinction between parallel branches does not fall within the focus of this work. Therefore, the correct detection of one of the indistinguishable parallel branches is treated as correct detection if one or more of these parallel branches are actually tripped.

The authors are aware of the fact that if all nodes of the network are monitored, the branches tripped can be derived without an optimizer by solving (2-3)

3. Implemented optimizing algorithm

The main challenges for the optimization are the high search space dimension equal to the number of branches of interest $\mathrm{L_{OI}}$ and the existence of multiple optimal solutions not linked to the actual outage event for a meshed network topology. The cause and effect of the multiple optimal solution are discussed subsequently. The general design approach avoids these challenges by the separation of $\Delta\mathbf{p}_{\mathrm{NL}}$ into two trial variables. The first – $\mathbf{x}_{\mathrm{B}}$ – is a vector which elements describe a subset of branches of interest. Only the branches in $\mathbf{x}_{\mathrm{B}}$ are considered as candidates for an outage. The number of branches in $\mathbf{x}_{\mathrm{B}}$ determines the search space dimension. The second – $\mathbf{x}_{\mathrm{P}}$ – is also a vector and its elements correspond to the amount of fictional power injections on the terminals of the candidate branches in $\mathbf{x}_{\mathrm{B}}$. The resulting two variable objective function is given as

$$f(\mathbf{x}_{\mathrm{B}},\mathbf{x}_{\mathrm{P}}) = \left\|\Delta\boldsymbol{\vartheta}_{\mathrm{meas}} - \mathbf{A}_{\mathrm{PMU}}\cdot\mathbf{K}_{\mathrm{D}}\cdot\mathbf{A}_{\mathrm{LOI}}(\mathbf{x}_{\mathrm{B}})\cdot\mathbf{x}_{\mathrm{P}}\right\|^2 \tag{3-1}$$

$$\mathbf{K}_{x_B} = \mathbf{A}_{\mathrm{PMU}}\cdot\mathbf{K}_{\mathrm{D}}\cdot\mathbf{A}_{\mathrm{LOI}}(\mathbf{x}_{\mathrm{B}}) \tag{3-2}$$

$\mathbf{A}_{\mathrm{PMU}}$	PMU incidence matrix
$\mathbf{A}_{\mathrm{LOI}}(\mathbf{x}_{\mathrm{B}})$	notation for columns corresponding to $\mathbf{x}_{\mathrm{B}}$ of the branch of interest incidence matrix $\mathbf{A}_{\mathrm{LOI}}$
$\mathbf{K}_{\mathrm{D}}$	complete correlation matrix between node power injection and node voltage angle change
$\boldsymbol{K}_{x_B}$	correlation matrix between trial variable $\mathbf{x}_{\mathrm{P}}$ and measured node voltage angles

The resulting matrix linking $\mathbf{x}_{\mathrm{P}}$ to $\Delta\boldsymbol{\vartheta}_{\mathrm{meas}}$ is further defined as $\mathbf{K}_{x_B}$ for simplified notation. Analyzing the objective function separately for each trial variable, it is obvious that a change in $\mathbf{x}_{\mathrm{B}}$ results in a discontinuous change in $\mathbf{K}_{x_B}$ and, consequently, altering the objective function's form. However, the objective function is continuous to changes in $\mathbf{x}_{\mathrm{P}}$ for any given $\mathbf{x}_{\mathrm{B}}$.

Based on this general behaviour towards the trial variables, a two level optimizer HPN is proposed, combining particle swarm optimization PSO [24] and Newton's method [25]. The outer level applies PSO on $\mathbf{x}_{\mathrm{B}}$ to define a continuous objective function f_{N} (3-3). f_{N} is the input for the inner level Newton's algorithm minimizing with respect to $\mathbf{x}_{\mathrm{P}}$. The minimal function value of f_{N} is handed back to the PSO as the function value of $\mathrm{f_{PSO}}$ (3-4) for the current value of $\mathbf{x}_{\mathrm{B}}$.

$$f_{\mathrm{N}}(\mathbf{x}_{\mathrm{P}}) = \left\|\Delta\boldsymbol{\vartheta}_{\mathrm{meas}} - \mathbf{K}_{x_B}\cdot\mathbf{x}_{\mathrm{P}}\right\|^2 \tag{3-3}$$

$$f_{\mathrm{PSO}}(\mathbf{x}_{\mathrm{B}}) = \min\left(f_{\mathrm{N}}(\mathbf{x}_{\mathrm{P}})_{\mathbf{x}_{\mathrm{B}}}\right) \tag{3-4}$$

The value of $\mathbf{x}_{\mathrm{B}}$ is the position of the PSO particle at the current iteration step. At each iteration step i, the position and velocity $\mathbf{v}_{\mathrm{B}}$ of the particle are updated as follows:

$$\mathbf{v}_{\mathrm{B}}^{(\mathrm{i}+1)} = w\cdot\mathbf{v}_{\mathrm{B}}^{(\mathrm{i})} + c_1\cdot r_1\cdot\left(\mathbf{p}_{\mathrm{p}} - \mathbf{x}_{\mathrm{B}}^{(\mathrm{i})}\right) + c_2\cdot r_2\cdot\left(\mathbf{p}_{\mathrm{g}} - \mathbf{x}_{\mathrm{B}}^{(\mathrm{i})}\right) \tag{3-5}$$

$$\mathbf{x}_{\mathrm{B}}^{(\mathrm{i}+1)} = \mathbf{x}_{\mathrm{B}}^{(\mathrm{i})} + \mathbf{v}_{\mathrm{B}}^{(\mathrm{i}+1)} \tag{3-6}$$

With these update formulas, the standard PSO with inertia weight and constrictions is implemented as described in [26]. Violations of search space limitations – minimum and maximum values of $\mathbf{x}_{\mathrm{B}}$ – are treated by setting the value to the closest limitation. This version of PSO is chosen, since it is widely known and its simple straight forward implementation allows a good evaluation of the usability of PSO for the given optimization problem. However, implementing more advanced PSO versions, e. g. as described in [27,28], might improve the results.

Since $\mathbf{x}_{\mathrm{B}}$ represents the selected candidate branches, the values in each of its dimensions must be discrete integers between 1 and the

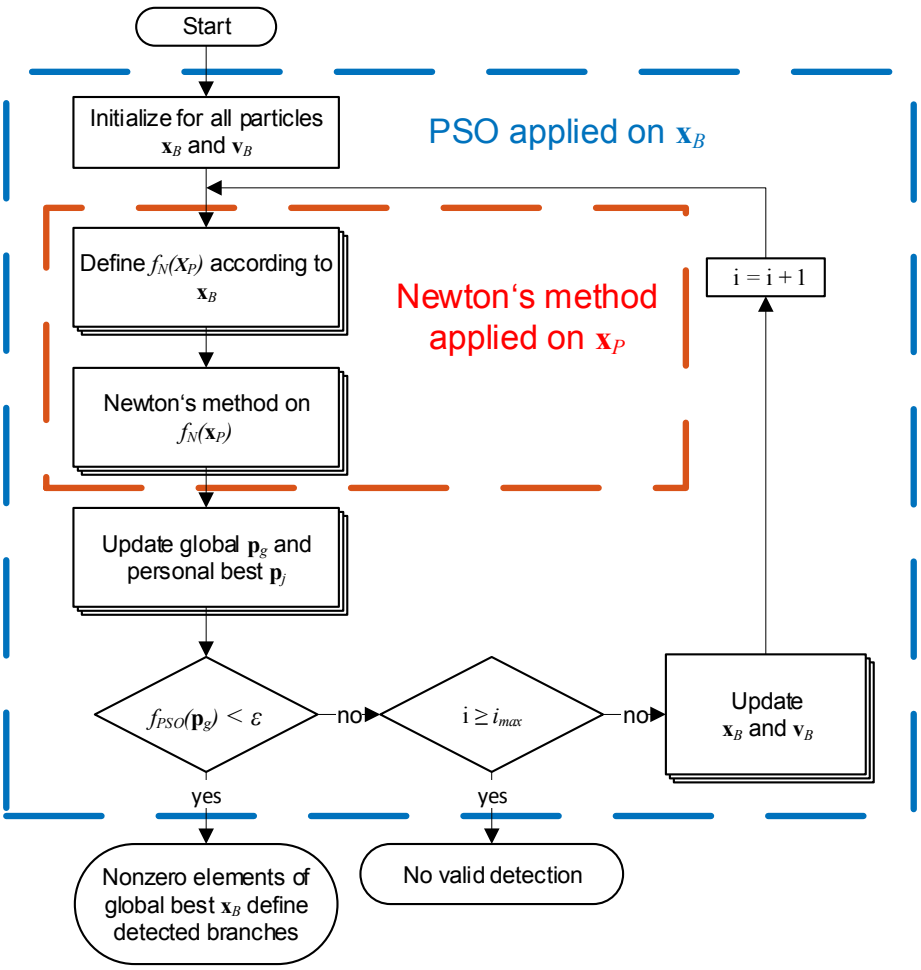

Fig. 3-1. Flow chart of the HPN based on a superordinate PSO and Newton's method.

number of branches in the network L. However, it is obvious that the stated update formulas of PSO lead to continuous values of $\mathbf{x}_B$ and it must be discretized with the prerequisite of equally large intervals.

The personal and global best position store the values of the particle's $\mathbf{x}_B$ leading to the smallest function value of f_{PSO}. The function value of f_{PSO} decreases if branches topologically close to the actually tripped branches are included in the branches of $\mathbf{x}_B$. The function value of f_{PSO} only becomes 0 or satisfies a $< \varepsilon$ condition if the tripped branches are part of the branches of $\mathbf{x}_B$. Therefore, a higher dimension of $\mathbf{x}_B$ – in other words more candidate branches per particle – has the effect of a faster convergence at the cost of detection accuracy. The decrease in the detection accuracy is caused by the possibility of multiple minima as soon as the branches in $\mathbf{x}_B$ form a meshed structure.

The gradient ∇f_N and Hessian $\mathbf{H}$ – needed to calculate the Newton step $\boldsymbol{\delta}$ (3-7) – are given by the Eqs. (3-8) and (3-9). If the second order minimization condition – the Hessian has to be positive definite – is violated, the method of Levenberg-Marquardt [29,30] is applied to assure a downhill direction of the Newton step.

$$\boldsymbol{\delta}(\mathbf{x}_P) = -\mathbf{H}^{-1} \cdot \nabla f_N(\mathbf{x}_P) \tag{3-7}$$

$$\nabla f_N(\mathbf{x}_P) = -2 \cdot \mathbf{K}_{x_B}^T \cdot (\boldsymbol{\vartheta}_{meas} - \mathbf{K}_{x_B} \cdot \mathbf{x}_P) \tag{3-8}$$

$$\mathbf{H} = 2 \cdot \mathbf{K}_{x_B}^T \cdot \mathbf{K}_{x_B} \tag{3-9}$$

Due to the optimizer's two-level approach, the Eqs. (3-7)–(3-9) must be evaluated at each PSO iteration step and for each particle separately at each. However, since the reduction of the matrix $\mathbf{K}_D$ to $\mathbf{K}_{x_B}$ as well as the calculation of ∇f_N and $\mathbf{H}$ are simple matrix multiplications, it is not computationally expensive. The inverse of $\mathbf{H}$ is constant for the iterations of Newton's method and therefore, must be calculated only once per PSO iteration step and particle.

The PSO's iteration is stopped, if $f_{PSO}(\mathbf{x}_B)$ satisfies a $< \varepsilon$ condition or the maximum number of iterations is reached. If a $< \varepsilon$ condition is satisfied, it is assumed that all tripped branches are within the corresponding $\mathbf{x}_B$. If the algorithm is aborted due to maximum iterations, the output is marked as not valid. The HPN's flowchart is shown in Fig. 3-1.

4. Application to Nordic-32-Bus system

4.1. Network settings and pre-evaluation

A variant of the Nordic-32-Bus system, as seen in Fig. 4-1, implemented and validated in DigSILENT is used. The model has been generously provided by the authors of [31]. The system mainly consists of 32 nodes representing a transmission grid with the nominal voltages of 400 kV (nodes 40xx), 220 kV (nodes 20xx) and 130 kV (nodes 10xx). The generators and loads are connected to the network with 22 additional medium voltage nodes. The dynamic model includes automatic voltage regulators, over excitation limiters and power system stabilizers as well as a frequency control and saturation effects for the generators. The voltage dependency of loads is modelled by equipping all load transformers with on load tap changers. The referenced branch numeration for the transmission lines and transformers are given in the appendix Table 8-1.

The base model is expanded with a VSC-HVDC link between the nodes 4042 and 4045 and simplified PMU models at the 400-kV-nodes.

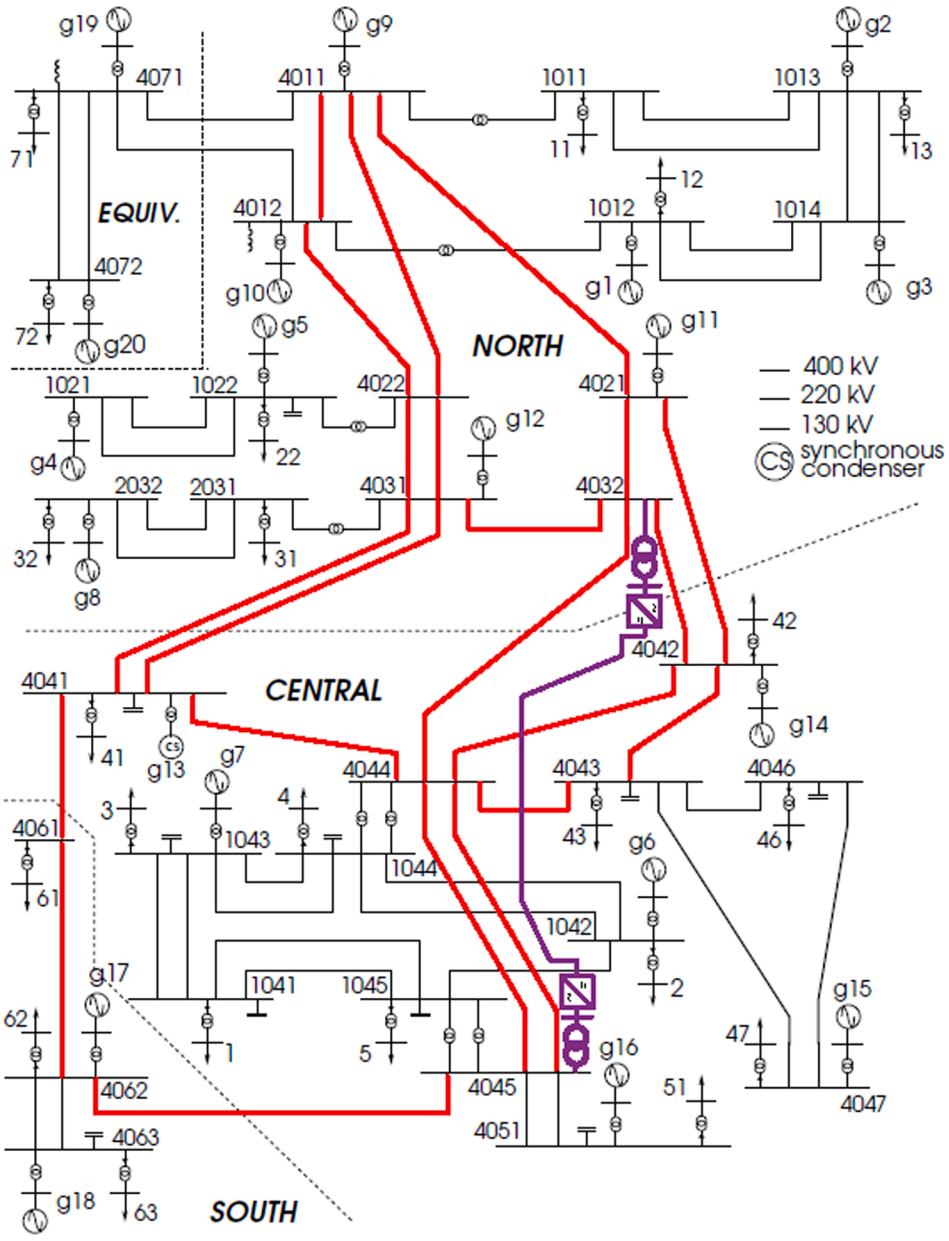

Fig. 4-1. Nordic-32-Bus single line diagram [32] with HVDC link (violet) and branches of interest (red).

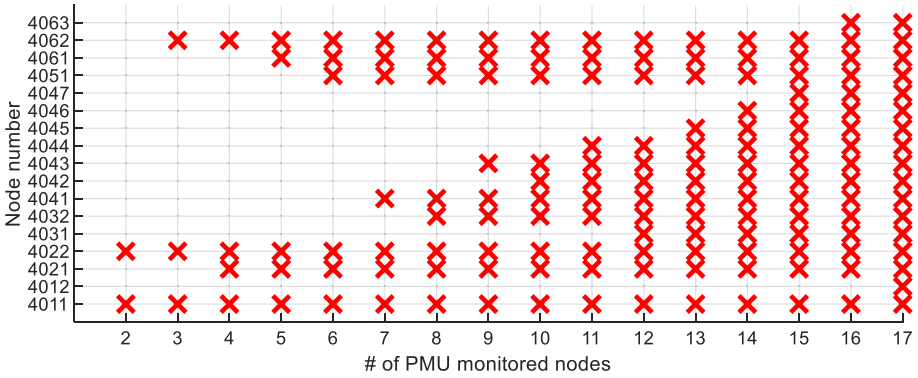

Fig. 4-2. Placement of PMU monitored nodes.

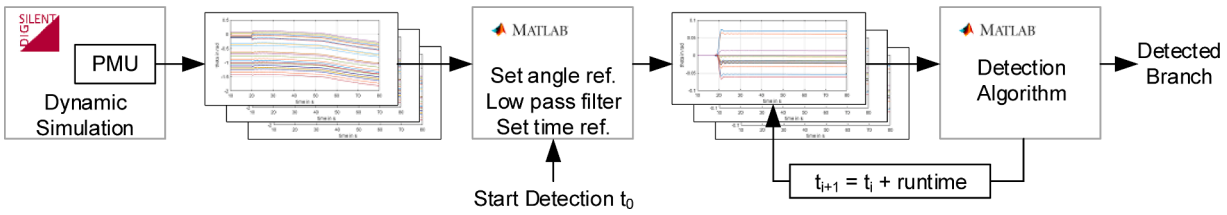

Fig. 4-3. Test process of the detection algorithms with dynamic simulation data.

The HVDC's location is chosen according to [20] to represent the DC link part of the south-west link currently under construction [33]. The branches of interest – marked red in Fig. 4-1 – were selected in a pre-evaluation based on the HVDC's expected effects on the branch loading and loading changes due to branch outages. The resulting branches of interest are {20, 21, 22, 24, 26, 27, 28, 29, 30, 31, 32, 33, 34, 35, 36, 37, 38, 39, 42, 43, 46, 48}.

In order to select the PMU monitored nodes, a pre-evaluation is conducted. The goal of the evaluation was to find the node combinations of the 400-kV-nodes with the highest amount of non-redundant information in the node voltage angle change for a given number of monitored nodes. The scalar product between the vectors corresponding to voltage angle changes in each node for each single branch of interest outage serves as a measure for the redundancy of information. The result of the pre-evaluation is shown in Fig. 4-2. The red x-marks indicate the PMU monitored nodes.

4.2. DC load flow simulation

Simulations with the linearized DC load flow model are used to evaluate the general robustness of the detection algorithm against a variation of the search space dimension, missing information and changed load flow situations. The DC load flow is used for this purpose, since the detection algorithm is based on it. Therefore, the ideal solution is known beforehand and errors due to the linearization do not exist. The linearized DC load flow model of the Nordic-32 Bus system contains only the 32 transmission system nodes, whereby node 4032 is set as the slack node. The loads and generation are shifted from the medium voltage nodes to the corresponding transmission system nodes.

The node voltage angle changes are calculated for each branch outage combination as follows, whereby the index b refers to the network before any branch tripping and index c to the network without the tripped branches. $\mathbf{B}_c$ and $\mathbf{B}_b$ are the corresponding system susceptance matrixes. The calculated node voltage angle changes are used as measurement input for the detection algorithm.

$$\Delta\boldsymbol{\vartheta} = \left(\mathbf{B}_c^{-1} - \mathbf{B}_b^{-1}\right) \cdot \left(\mathbf{p}_{gen} - \mathbf{p}_{load}\right) \tag{4-1}$$

The generation and load data are varied over 1000 load cases to ensure a load flow independent performance test. The distribution is achieved by assigning a uniformly distributed number between 0 and 1 to the corresponding nodes and subsequently scaling to the total network load. The detection performance is then statistically evaluated for all possible single and double branch outages. Significant cases – original load data, worst, mean and best detection ratio – are used for testing the principal applicability of the algorithm on triple branch outages.

This evaluation is important for a better understanding of the algorithm's principal behaviour and dependencies without additional error sources such as linearization error, controller actions and oscillations.

4.3. Dynamic simulations

The algorithms' real-world applicability is evaluated by dynamic simulations taking oscillations and control actions into account. The angle changes are derived from a dynamic simulation performed with *DigSilent PowerFactory* [34]. Fig. 4-3 shows the test process from the dynamic simulation to the actual detector implemented as MATLAB script.

The PMU data is the detector's measurement input data stream. The detector applies simple data pre-processing, such as a low pass filter and referencing the measured voltage angles to the reference bus. The detection algorithm is started manually after the outage occurs and is executed repeatedly for 10 s. The start can be automated, e.g., by applying edge detection algorithms as suggested in [5]. However, this falls outside the focus of this work. The change in the node voltage angle is calculated with respect to fixed reference values which are measured 10 s before the contingency event. Oscillations triggered by the branch tripping and linearization errors of the objective function can cause different detection results for the individual detection runs. Therefore, the output of the detection process is the branch or branch combination which has the highest overall appearance in the results of the detection runs within the runtime window of 10 s. Detection runs without the optimizer's convergence are included as empty results for the calculation of the appearance. To increase the reliability of the detection, a branch is only marked as tripped if a minimum detection threshold ξ, e.g., 0.4 pu appearance of all detection runs including empty results – is exceeded. The effects and interpretation of this threshold value are discussed in 5.2.2.

The function diagram of the implemented PMU model is shown in Fig. 4-4. The available input is the frequency in pu as well as the sine and

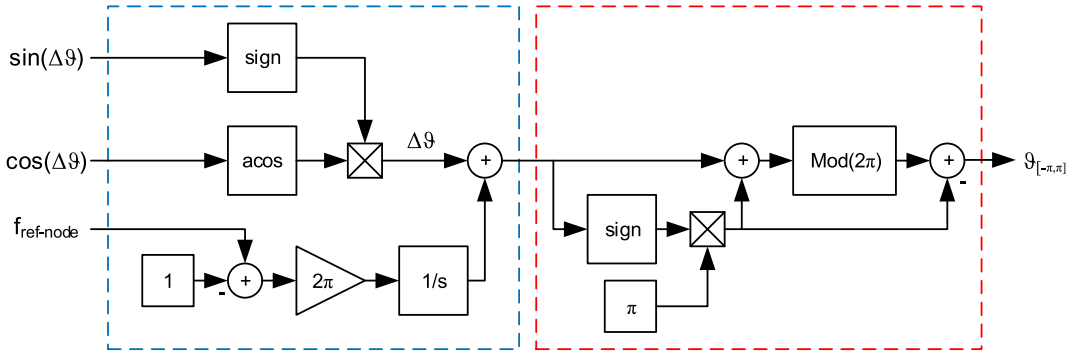

Fig. 4-4. PMU measured node voltage angle model.

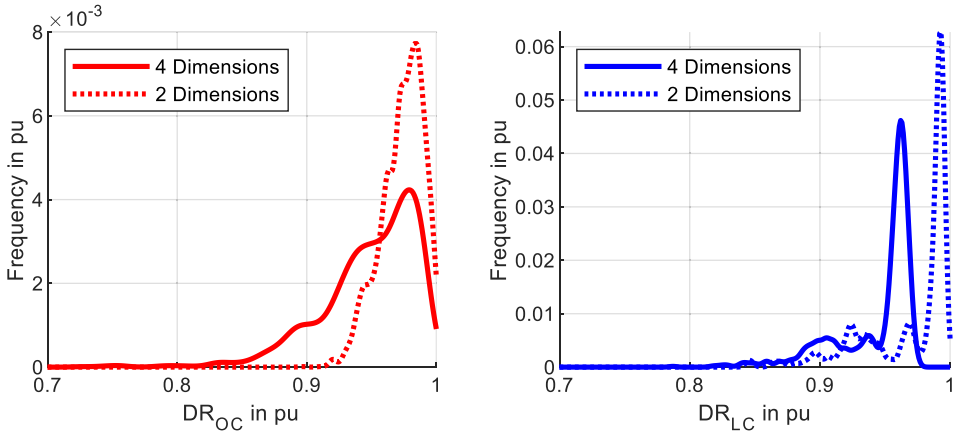

Fig. 5-1. Frequency of correct detection ratio estimated using KDE.

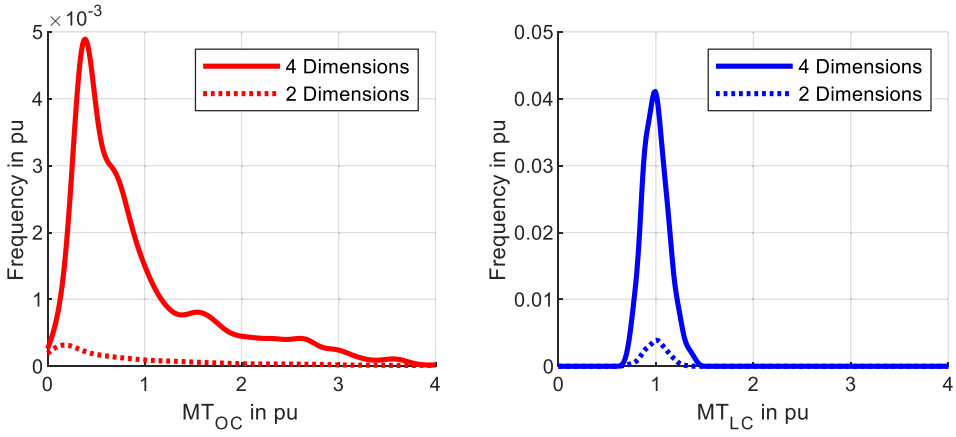

Fig. 5-2. Frequency of the detection run time estimated using KDE. The detection run time is referred to its mean value to allow a comparison between 2- and 4-dimensional search spaces.

cosine of the angle difference $\Delta\vartheta$ between the slack node and the PMU monitored node. $\Delta\vartheta$ in radiant and its sign are calculated from the sine and cosine information. The frequency deviation from the nominal value is multiplied with 2π and integrated to calculate the frequency depending angle drift of the reference node to the fictive global angle reference. The unrestrained node voltage angle of the measured node is derived from the sum of $\Delta\vartheta$ and angle difference of the reference node to the global angle reference. The result is processed further in the portion marked in red to limit the angle to a range between -π and π.

5. Results

5.1. Evaluation of linearized DC load flow simulations

The main performance parameters for the detection algorithm are the detection ratio, the detection runtime and its vulnerability to missing node information. The evaluation is conducted for the detection results of the 1000 load cases, which are created as described in 4.2. The detection algorithm is implemented as a MATLAB script and will run on one core of an i7-4790 3.60 GHz CPU.

The correct detection ratio (DR) and mean detection run time (MT) are evaluated for two options:

- The index $_{OC}$ refers to the simulation results of a specific branch outage combination which is evaluated for all 1000 load cases with Eq. (5-1).
- The index $_{LC}$ refers to the simulation results of a specific load case which is evaluated for all possible branch outage combinations with Eq. (5-2).

$$\begin{aligned} DR_{OC} &= \frac{\#correct_{OC}}{\#load\ cases} \\ MT_{OC} &= \frac{\sum RT_{OC}}{\#load\ cases} \end{aligned} \tag{5-1}$$

$$\begin{aligned} DR_{LC} &= \frac{\#correct_{LC}}{\#outage\ combinations} \\ MT_{LC} &= \frac{\sum RT_{LC}}{\#outage\ combinations} \end{aligned} \tag{5-2}$$

RT	detection run time of a single contingency event
#correct	number of correct detections per outage combination ($_{OC}$) or per load case ($_{LC}$)
#load cases	number of simulated load cases (1000)
#outage combinations	number of feasible double branch outage combinations (3336)

The following visualizations of these evaluations for the detection results based on node voltage angle information of all 32 nodes uses the kernel density estimation (KDE) based on normal distribution, see Figs. 5-1 and 5-2. The search space dimensions of 2 and 4 are chosen to show the result dependency based on the minimal search space and a sufficient larger search space. The KDE parameters are derived using the

Table 5-1
Correct detection ratio and detection run time.

		4-dimensional search space		2-dimensional search space	
		OC	LC	OC	LC
DR in pu	Worst	0.257	0.787	0.193	0.845
	Mean	0.944		0.969	
	Best	1.0	0.975	1.0	0.998
	Mode	0.979	0.962	0.984	0.993
MT in ms	Minimum	7.7	52.1	7.0	622.0
	Mean	74.5		899.1	
	Maximum	398.6	105.0	6771.9	1186.9
	Mode	29.0	74.0	155.0	905.0

MATLAB® function 'fitdist' [35]. The per unit reference for the resulting frequency of DR_{OC} and MT_{OC} is 3336, which is the number of single and double branch outage combinations not leading to islanding of network parts and 1000 for DR_{LC} and MT_{LC}. The frequency is interpreted as the relative appearance of the value on the abscissa. E.g., a frequency of 0.001 pu at a DR_{OC} of 0.9 pu means that 0.001 pu of all possible branch outage combinations have a DR_{OC} of 0.9 pu).

The frequency of DR_{OC} in Fig. 5-1 shows significant saddles at detection ratios around 0.9 pu and 0.95 pu as well as a relative exposed mode at 0.98 pu for a 4-dimensional search space. The two saddles are caused by topological issues and mainly correspond to three-branch loops, whereby the worst detection ratio occurs for branches participating in more than one three-branch loop. The branch with the smallest impedance in any of the loops is more often wrongly detected, since higher node power injections are necessary to obtain the measured change in node voltage angle. The higher number of wrong detections for these branches results from the tendency of the Newton part optimizing algorithm to find a solution closest to the initial point. The results for the reduced search space dimension to 2 supports this conclusion on the topological effect. Consequently, three-branch loops no longer lead to wrong detection results, since they simply no longer exist in the optimizers search space. That leads to a probability density function with a more pronounced mode. The remaining small saddles are caused by 400-kV-branches in parallel to network parts of lower voltage.

Focusing on the frequency of DR_{LC} in Fig. 5-1 enables conclusions to be drawn on the influence of the load flow situation on the detection ratio. The dominant mode occurring in the data for 2- and 4-dimensional search space indicates a robustness of the detection algorithm against different load flow situations. The smaller peaks which start to occur at about 0.9 pu detection ratio might be caused by the stochastic PSO part of the HPN.

The frequencies of the mean detection run time *MT*, depicted in Fig. 5-2, similarly show a stronger influence of the network topology on the detector performance. The mean detection run time on the abscissa is referred to its mean value – 74.3 ms for the 4-dimensional search space and 899 ms for the 2-dimensional search space– to allow a comparison between the search space dimensions in one graph.

Focusing on the results of the 4-dimensional search space first, the mode of MT_{OC} occurs for a detection run time of 29 ms – or 0.39 pu – and has right side skewed behaviour which is caused by a small number of outage combinations with higher detection run times. MT_{LC} has its mode at a detection run time of 74 ms – or 0.99 pu. Its sharp and nearly symmetrical shape indicates only a minor influence of the load flow situation on the detection run time. The evaluations for the 2-dimensional search space have a much flatter frequency profile for both MT_{out} and MT_{LC} which indicates a greater scattering of the results. However, the principle shape of the frequency profile is comparable between 2- and 4-dimensional search spaces. These observations match with the conclusions drawn from evaluations of the correct detection ratio.

Table 5-2
Detection ratio DR_{LC} and mean detection run time MT_{LC} for the outage of three branches.

		2 branch out	3 branch out
DR_{LC} in pu	Worst	0.787	0.959
	Mean	0.944	0.983
	Best	0.975	0.981
	Original	0.944	0.938
MT_{LC} in ms	Worst	52.1	923
	Mean	68.6	900
	Best	105.0	912
	Original	59.2	1022

The main parameters of the result evaluation are summarized in Table 5-1. Comparing the mean correct detection ratio with the correct detection ratio corresponding to the mode, it becomes obvious that the resulting frequencies are left skewed independently of the search space. The mean detection run time is right skewed for the outage-based interpretation MT_{OC}, whereby the 2-dimensional application has a higher skewness. Summarizing the skewness, it shows that the expectable correct detection ratio is higher than the mean value of the correct detection ratio of the simulation results and has a shorter detection run time.

Comparing the results for 2- and 4-dimensional search spaces shows generally a slightly higher detection ratio for the 2-dimensional search space. The slight increase in the detection ratio comes at the cost of a significant increase in the detection run time. Both effects are explained as follows. An increase in the search space dimensions allows the algorithm to check more branch combinations at each iteration, thus reducing detection run time. However, the increase in the dimension also leads to an increased probability of loops in the selected candidate branches, including the actual tripped branches causing wrong detections.

A comparison to the mean values of the detection ratio and detection runtime obtained by applying PSO on both types of the separated trial variables ($DR_2 = 0.936$, $DR_4 = 0.2$, $MT_2 = 354$ ms, $MT_4 = 959$ ms) shows clearly the improvements achieved with the introduction of the HPN algorithm. PSO performs comparably well for small search space dimensions but is not suitable for larger search space dimensions due to unacceptable low detection ratios and high detection run times. Applying PSO without a separation of the trial variables does not yield useful results. Based on these findings and conducted pre-evaluations on dynamic simulation data, the PSO is not further investigated in this work.

Based on the results of double branch outage detection, the original load case as well as the load cases corresponding to the worst, closest to the mean and best load DR_{LC}, are selected to test the algorithm on the detection of three branch outages. This reduction in evaluated cases is due to limit the simulation's run time to a reasonable time span. In Table 5-2, the mean detection ratio and detection run time are stated for the four load flow samples.

The number of maximal detectable branches and actually tripped branches differs less. Therefore, the possibility of combinations that lead to an optimal minimum of the objective function not linked to the branches tripped decreases and the detection ratio increases. The distribution of the detection ratio is not linked to the results of the double branch outages. This indicates again that the actual pre-contingency load flow has smaller influence on the algorithm's performance than

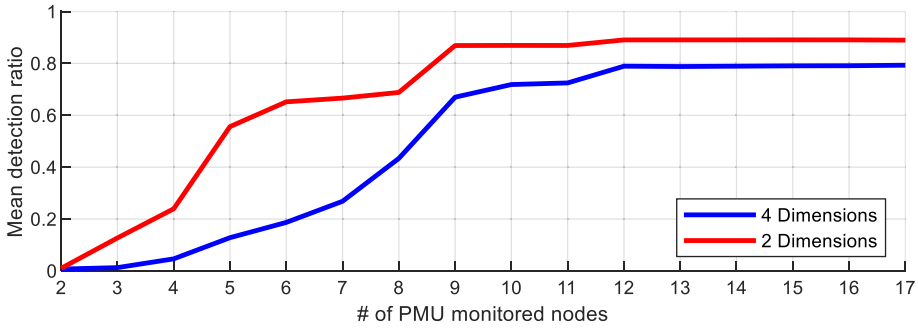

Fig. 5-3. HPN's mean detection ratio for a double branch outage with different numbers of PMU monitored nodes.

Table 5-3
Optimizer parametrization used for the evaluation of linearized data.

w	c_1	c_2	Search space dimension	i_{max}	#particles
1 … 0.3	1.05	1.05	2	500	20
1 … 0.3	1.05	1.05	4	500	40

the topology.

A reduction in the number of PMU monitored nodes decreases the input information of the algorithms. In the following, the HPN's detection performance is assessed using node sets with an increasing number of monitored nodes – see Fig. 4-2 – for outage combination of the branch set stated in Section 4.1. The evaluation is conducted for a search space dimension of 2 and 4. The depicted mean detection ratio refers to the mean value over all outage combinations and load cases. As can be seen in Fig. 5-3, an increase in the search space dimension leads to a higher decreasing effect in the detection ratio.

The algorithm's parameters used in this section are given in Table 5-3.

5.2. Evaluation of dynamic simulation data

The applicability of the HPN-based detection methodology in real systems is tested with PMU data from dynamic simulations. The evaluation is separated into considerations for single branch outages focusing on the detection performance for reduced monitored nodes and considerations for double branch outages. Furthermore, for the single branch outages, a comparison of the detector's detection ratio with the results for an analytical method based on [5,6] is completed, whereby no validation check using a maximum distance criterion is used for the analytical methods.

The optimizer's DC load flow model network representation leads to an immanent linearization error. The optimizer reacts to this by adding small unnecessary power injections at terminal nodes of branches not tripped, consequently causing more non-zero elements to define the detected branches. This effect is avoided by implementing a minimum value for the power injections to be taken into account. Since their actual values depend on the pre-contingency load flow, the minimum value is referenced to the maximum power injection of the optimizer output. In the following, a cut off ratio of 0.2 pu is used as the referenced minimum power injection value. Due to this, the detection algorithm only considers power injections higher than 0.2 times the maximum power injection for the output selection of the tripped branches.

Additionally, the linearization errors affect the selection of a sensible value for the optimization tolerance ε, used as stopping criterion. For the following evaluations, ε values of 0.005 rad and 0.02 rad are implemented. However, an optimal selection of the value ε also depends on the chosen search space dimension and the network topology. Therefore, the search space dimensions with values of 3 and 4 are evaluated.

Table 5-4 summarizes the different parameter sets of the HPN evaluated in the following.

The set of branches and PMU monitored nodes used for the evaluations are provided in Section 4.

5.3. Single branch outage

The generation and load parameters remain unchanged for the simulation of the single branch outages from the original data from [31]. The branch number 21 – the line connecting nodes 4011 and 4021 – is additionally excluded from the set of evaluated branch outages defined by the indices stated in Section 4.1, since its outage leads to a voltage instability followed by a loss of synchronization of the generators in the central and south parts of the grid.

Fig. 5-4 shows the correct detection ratio over the number PMU monitored nodes and for different HPN parametrization. The detection threshold ξ in the output appearance for a valid detection result is set to 0.4 pu. The graphs indicate a higher robustness against missing node information with lower search space dimensions, which is reasonable in view of reduced probability of loop structures in the selected candidate branches. The chosen value for ε has only a minor influence on the detection ratio.

The influence of the threshold ξ on the correct detection is depicted in Fig. 5-5, whereby the HPN output data for a search space dimension of 3 and an ε of 0.005 rad is selected for representation. The detection results of an analytical detection algorithm similar to [5,6] are included for comparison in the figure. However, the detection performance of the analytical algorithm might be overrated, since no validation check as described in [5] and no threshold ξ on the appearance ratio as for the HPN are included. Due to the missing thresholds, the equivalent in the HPN data for a comparison is the green graph for a $\xi = 0$ pu. Only correct or wrong results exist for a detection threshold of $\xi = 0$ pu. These results are linked to the element with the highest absolute appearance in the detector output stream without any threshold and reflect the maximal reachable ratios. A comparison of these two graphs shows that the HPN performance is equal or slightly better in means of average detection ratio for 5 or more PMU monitored nodes.

Table 5-4
Optimizer parametrization used for the evaluation of dynamic data.

w	c_1	c_2	Search space dimension	ε	Cut off ratio	i_{max}	#particles
1 … 0.3	1.05	1.05	3	0.005	0.2	1000	30
1 … 0.3	1.05	1.05	3	0.02	0.2	1000	30
1 … 0.3	1.05	1.05	4	0.005	0.2	1000	40
1 … 0.3	1.05	1.05	4	0.02	0.2	1000	40

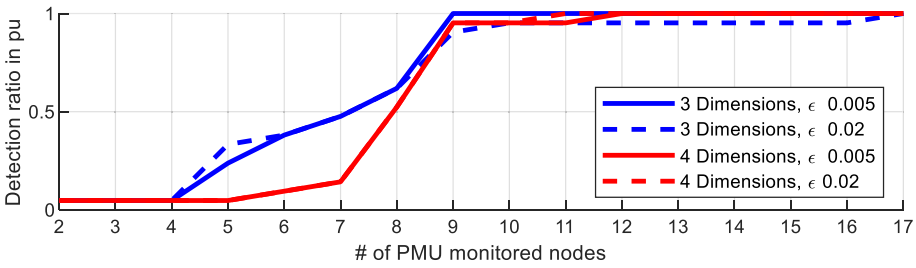

Fig. 5-4. Detection ratio for reduced number PMU monitored nodes for different parametrization and $\xi = 0.4$ pu.

However, for $\xi = 0$ pu a single detected element would be interpreted as the solution if it is the only non-empty detection output. With increasing detection threshold values, the detection results become more and more reliable. The decreasing detection ratio with higher detection threshold values is caused by increasing numbers of no-result outputs of the detector. Wrong detections definitely decrease similarly to increasing detection thresholds.

The detection run time of the HPN algorithm naturally depends on the available node information, the search space dimension and the chosen ε, whereby these factors are listed according to their severances. Due to the wide range in the detection run time starting from around 350 ms for 2 monitored nodes and going below 5 ms for 17 monitored nodes, a graphical presentation is set aside. However, the detection run time is well below 50 ms for the numbers of monitored nodes enabling reasonably good detection ratios. This short run times allow enough optimization runs in the 10 s detection window to have a solid decision base.

5.4. Double branch outage

The loading of the used Nordic-32-Bus system is scaled down to 70% of the original load data from [31] to enable a stable post contingency state of the double branch outages. However, some outage combinations still have no stable solution – mainly combinations including branch 21. These instable outage combinations and outage combinations leading to the islanding of network parts are not included in the results. This leaves a set of 226 simulated branch outages defining the node voltage angle data for the evaluation of the detection algorithm.

Fig. 5-6 shows the correct detection results on dynamic data for an HPN parametrization with a search space dimension of 4 and an ε of 0.005 rad. All 17 400-kV-nodes are considered as PMU monitored and the detection threshold ξ is set to 0.5 pu. The green squares indicate a correct detection of the outage combination – the correct combination has an appearance in the output data of the 10 s detection window higher than ξ. The red squares indicate a wrong detection – a wrong output combination has an appearance higher than ξ. The blue squares indicate no detection result – neither a correct nor a wrong combination has an appearance higher than ξ. The black squares reference branch outages either resulting in the islanding of network parts or causing instabilities. The wrong detections are concentrated on combinations including the branches 30, 33 and 48. This is caused for the branches 30 and 33 by their topology-based probability to be the lowest impedance branch of a loop formed by the optimizer's candidate branches and the higher likeliness of wrong detection linked to that. The tripping of branch 48 leads to strong oscillations of the generators g17 and g18 and therefore causes the wrong detection results.

The influence of the chosen value of ξ on the overall detection ratio of double branch outages for different values of ε and a search space dimension of 4 are given in Fig. 5-7. The graphs depict the ratios of correct, wrong and no detection for HPN as a function of the detection threshold ξ and 17 PMU monitored nodes. The maximum correct detection ratio is 0.91 pu. The correct detection ratio slowly decreases and forms a knee point at $\xi = 0.6$ pu. The ratio of no results becomes dominant while the correct and wrong detection ratio decreases to

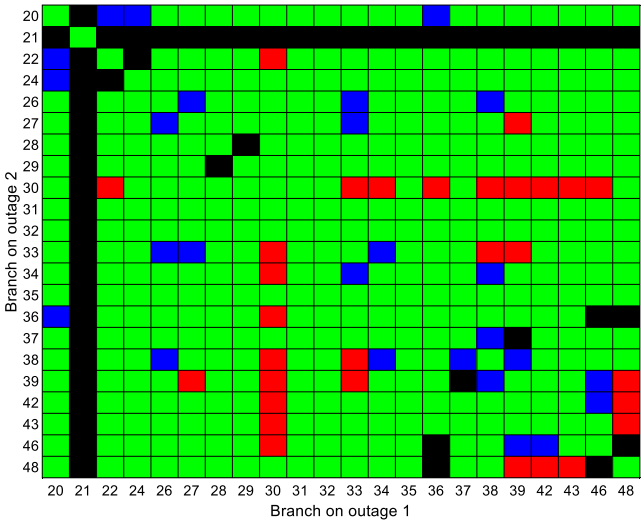

Fig. 5-6. Detection result for a search space dimension of 4, ε of 0.005 pu, ξ = 0.5 pu and 17 PMU monitored nodes. Green correct detection, red wrong detection, blue no detection, black not evaluated.

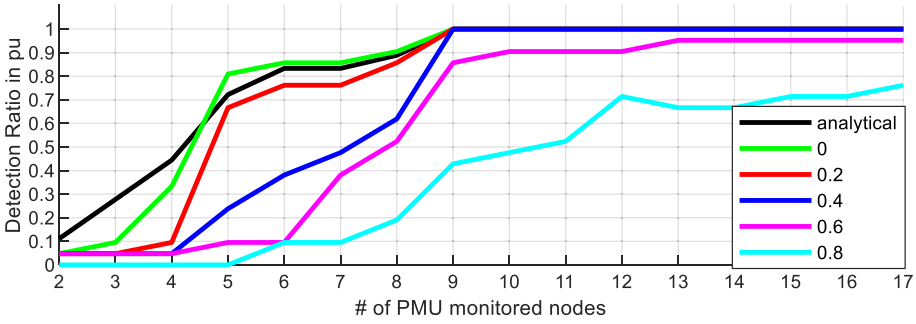

Fig. 5-5. Detection ratio for reduced number of PMU monitored nodes for different ξ values and an HPN parametrization with search dimension 4 and ε of 0.005 rad.

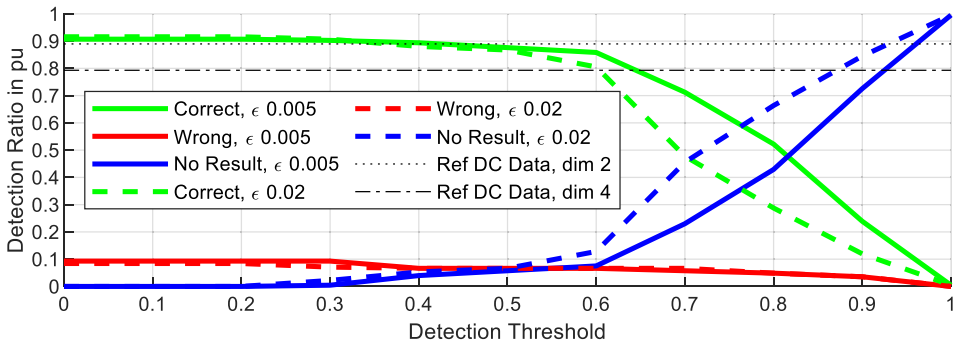

Fig. 5-7. Dependency on threshold for HPN with a search space dimension of 4 on dynamic simulation data for 17 PMU monitored nodes.

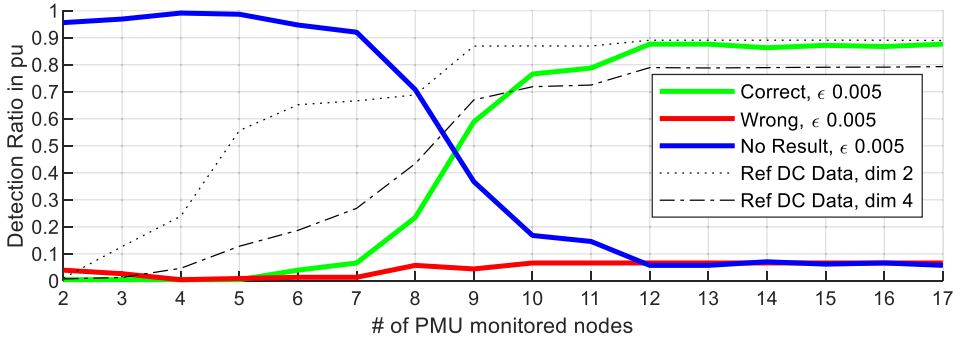

Fig. 5-8. Detection ratio of HPN with a search space dimension of 4, ε of 0.005 pu, $\xi = 0.5$ pu for dynamic simulation data.

0 with further increasing threshold values, whereby the smaller ε of 0.005 pu enables higher correct detection ratios.

The comparison to the reference detection ratio obtained from the evaluations of the linearized load flow calculations show that the algorithm is performing similarly well on the dynamic data till the knee point at $\xi = 0.6$ pu.

In Fig. 5-8 the dependency of the HPN's detection ratio on the number of PMU monitored nodes is depicted for a parametrization with 4-dimensional search space, an ε of 0.005 pu and a threshold of 0.5 pu. The general dependency of the correct detection ratio behaves similarly to correct detection ratio for the single branch outage – Fig. 5-4. The comparison with the reference detection ratios obtained from the evaluation of the linearized load flow data (Ref DC Data) shows that with higher numbers of monitored nodes, the influence of the linearization error of the optimizer's underlying model decreases. Furthermore, the graphs highlight that the detector has a constant low ratio in explicitly wrong detections.

The graphs in Fig. 5-9 show the dependency of the correct detection ratio on the chosen threshold and different parametrizations of the HPN. The value of ε is set to 0.005 pu and the search space dimension is 3 and 4, respectively. The black dotted and dash-dotted lines are the detection ratios obtained from the linearized load flow evaluations serve as reference. Comparing the detection ratios of the different search space dimensions and thresholds, it becomes notable that with smaller threshold values – 0 pu and 0.4 pu in the graph – and more than 9 observed nodes, a higher search space dimension yields a better detection ratio. This behaviour contradicts the expectation based on the results from the single branch evaluations. This is plausible by considering that the optimizer is able to compensate the linearization error better in a higher dimensional search space leading to a higher convergence rate and fewer empty results in the detection algorithm. With increasing threshold values, the detection ratio for the smaller search space

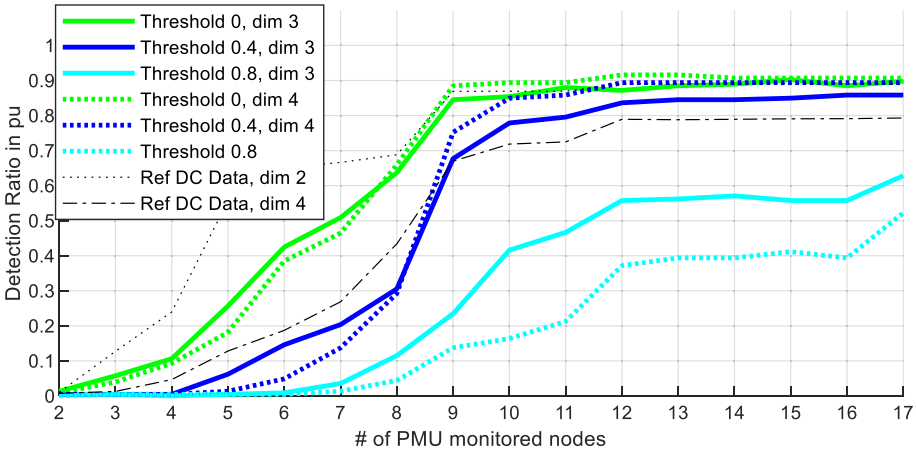

Fig. 5-9. Referenced detection ratio of HPN optimizer for reduced number PMU monitored nodes on dynamic simulation data with different thresholds.

dimension is better, since the actually detected branches for each individual detection run are more stable. This is caused by the lower probability of forming loops in the candidate branches. The same holds true for the detection ratio for numbers of observed nodes below 8. The probability of candidate branch loops dominates the decreasing effect for small numbers of observed nodes and higher threshold values. For lower threshold values, the linearization error has a stronger albeit decreasing impact for higher numbers of observed nodes.

The detection runtime for the double branch outages behave similarly to the detection runtime of the single branch outages. This means that enough detection runs are conducted in the 10 s detection window to have a solid decision base.

6. Conclusion

In this paper, an optimization-based approach for the detection of tripped branches is presented which requires only the node voltage angle information provided from PMU measurements. The proposed detection algorithm is able to detect multi-branch outages without extensive pre-calculations of possible outage combinations or a predefinition of the expected number of tripped branches.

The detection performance of the proposed algorithm is robust against the loss of node information as long as a certain number of measured nodes is not undershot. Focusing on the basic parametrization, the most critical parameter is the selection of the search space dimension, since it has a negative impact on the detection ratio if chosen to be too small or too large, depending on the network topology and the chosen detection threshold. The choice of the space dimension should consider the maximum sensible number of tripped branches – taking into account general network stability – as well as the linearization error of the underlying model. However, the results show that as long as the linearization assumptions are mostly met, the detection ratios achieved on the data created with the described dynamic nonlinear and stationary linear simulation models are comparable.

The number of explicitly wrong results over the whole range of evaluated threshold values and number of monitored nodes is small for the proposed algorithm. It is therefore a possible tool for future back-up monitoring applications and standalone emergency control actions of decentral resources. The next working steps are to test the detection algorithm on linearized and static AC load flow data of large systems such as the ENTSO-E network and on defining triggers for emergency control actions based on the detection output in dynamic simulations.

CRediT authorship contribution statement

Stefan Polster: Conceptualization, Methodology, Software, Formal analysis, Writing - original draft, Visualization, Funding acquisition. **Herwig Renner:** Conceptualization, Writing - review & editing, Supervision, Funding acquisition. **Robert Schürhuber:** Resources, Writing - review & editing, Supervision. **Katrin Friedl:** Writing - review & editing.

Declaration of Competing Interest

The authors declare that they have no known competing financial interests or personal relationships that could have appeared to influence the work reported in this paper.

Appendix A

See Table 8-1.

Table 8-1
Referenced branch numeration.

Nr.	Name	From node	To node	Type	Nr.	Name	From node	To node	Type
1	1011–1013	1011	1013	Line	**31**	4031–4041	4031	4041	Line
2	1011-1013b	1011	1013	Line	**32**	4031-4041b	4031	4041	Line
3	1012–1014	1012	1014	Line	**33**	4032–4042	4032	4042	Line
4	1012-1014b	1012	1014	Line	**34**	4032–4044	4032	4044	Line
5	1013–1014	1013	1014	Line	**35**	4041–4044	4041	4044	Line
6	1013-1014b	1013	1014	Line	**36**	4041–4061	4041	4061	Line
7	1021–1022	1021	1022	Line	**37**	4042–4043	4042	4043	Line
8	1021-1022b	1021	1022	Line	**38**	4042–4044	4042	4044	Line
9	1041–1043	1041	1043	Line	**39**	4043–4044	4043	4044	Line
10	1041-1043b	1041	1043	Line	**40**	4043–4046	4043	4046	Line
11	1041–1045	1041	1045	Line	**41**	4043–4047	4043	4047	Line
12	1041-1045b	1041	1045	Line	**42**	4044–4045	4044	4045	Line
13	1042–1044	1042	1044	Line	**43**	4044-4045b	4044	4045	Line
14	1042-1044b	1042	1044	Line	**44**	4045–4051	4045	4051	Line
15	1042–1045	1042	1045	Line	**45**	4045-4051b	4045	4051	Line
16	1043–1044	1043	1044	Line	**46**	4045–4062	4045	4062	Line
17	1043-1044b	1043	1044	Line	**47**	4046–4047	4046	4047	Line
18	2031–2032	2031	2032	Line	**48**	4061–4062	4061	4062	Line
19	2031-2032b	2031	2032	Line	**49**	4062–4063	4062	4063	Line
20	4011–4012	4011	4012	Line	**50**	4062-4063b	4062	4063	Line
21	4011–4021	4011	4021	Line	**51**	4071–4072	4071	4072	Line
22	4011–4022	4011	4022	Line	**52**	4071-4072b	4071	4072	Line
23	4011–4071	4011	4071	Line	**53**	1011–4011	1011	4011	Transf.
24	4012–4022	4012	4022	Line	**54**	1012–4012	1012	4012	Transf.
25	4012–4071	4012	4071	Line	**55**	1022–4022	1022	4022	Transf.
26	4021–4032	4021	4032	Line	**56**	2031–4031	2031	4031	Transf.
27	4021–4042	4021	4042	Line	**57**	1044–4044	1044	4044	Transf.
28	4022–4031	4022	4031	Line	**58**	1044-4044b	1044	4044	Transf.
29	4022-4031b	4022	4031	Line	**59**	1045–4045	1045	4045	Transf.
30	4031–4032	4031	4032	Line	**60**	1045-4045b	1045	4045	Transf.

References

[1] Zhao J, Antonio G, Netto M, Member S. Power system dynamic state estimation : IEEE task force on power system dynamic state and parameter estimation. IEEE Trans Power Syst 2019;34(4):3188–98. https://doi.org/10.1109/TPWRS.2019.2894769.

[2] James J, Bindu S. Hybrid state estimation including PMU measurements. 2015 Int. Conf. Control. Commun. Comput. India, ICCC 2015, no. November, pp. 309–313, 2016, doi: 10.1109/ICCC.2015.7432911.

[3] Farantatos E, Stefopoulos GK, Cokkinides GJ, Meliopoulos AP. PMU-based dynamic state estimation for electric power systems. 2009 IEEE Power Energy Soc Gen Meet PES 2009;'09:1–8. https://doi.org/10.1109/PES.2009.5275407.

[4] Zhao Y, Chen J, Goldsmith A, Poor HV. Identification of outages in power systems with uncertain states and optimal sensor locations. IEEE J Sel Top Signal Process 2014;8(6):1140–53. https://doi.org/10.1109/JSTSP.2014.2342191.

[5] Tate JE, Overbye TJ. Line outage detection using phasor angle measurements. IEEE Trans Power Syst Nov. 2008;23(4):1644–52. https://doi.org/10.1109/TPWRS.2008.2004826.

[6] Tate JE, Overbye TJ. Double line outage detection using phasor angle measurements. IEEE Trans Power Syst 2008;23(4):1644–52. https://doi.org/10.1109/TPWRS.2008.2004826.

[7] Sehwail H, Dobson I. Locating line outages in a specific area of a power system with synchrophasors. 2012 North Am Power Symp NAPS 2012;2012(2):1–6. https://doi.org/10.1109/NAPS.2012.6336315.

[8] Alam M, Mishra B, Thakur SS. A new approach of multiple line outage identification using phasor measurement unit (PMU) with bad data. Proc. 2018 Int. Conf. Curr. Trends Towar. Converging Technol. ICCTCT 2018, pp. 1–6, 2018, doi: 10.1109/ICCTCT.2018.8551021.

[9] Alam M, Kundu S, Thakur SS, Banerjee S. A new algorithm for single line outage estimation. Proc. 3rd Int. Conf. 2019 Devices Integr. Circuit, DevIC 2019, pp. 113–117, 2019, doi: 10.1109/DEVIC.2019.8783954.

[10] Sun K, Likhate S, Vittal V, Kolluri VS, Mandal S. An online dynamic security assessment scheme using phasor measurements and decision trees. IEEE Trans Power Syst 2007;22(4):1935–43. https://doi.org/10.1109/TPWRS.2007.908476.

[11] Zhu H, Giannakis GB. Sparse overcomplete representations for efficient identification of power line outages. IEEE Trans Power Syst 2012;27(4):2215–24. https://doi.org/10.1109/TPWRS.2012.2192142.

[12] Banerjee T, Chen YC, Dominguez-Garcia AD, Veeravalli VV. Power system line outage detection and identification - A quickest change detection approach. ICASSP, IEEE Int Conf Acoust Speech Signal Process - Proc 2014:3450–4. https://doi.org/10.1109/ICASSP.2014.6854241.

[13] Chen YC, Banerjee T, Dominguez-Garcia AD, Veeravalli VV. Quickest line outage detection and identification. IEEE Trans Power Syst 2016;31(1):749–58. https://doi.org/10.1109/TPWRS.2015.2394246.

[14] Rovatsos G, Jiang X, Domínguez-García AD, Veeravalli VV. Statistical power system line outage detection under transient dynamics. IEEE Trans Signal Process 2017;65(11):2787–97. https://doi.org/10.1109/TSP.2017.2673802.

[15] Jiang X, Chen YC, Veeravalli VV, Dominguez-Garcia AD. "Quickest line outage detection and identification: Measurement placement and system partitioning. 2017 North Am Power Symp NAPS 2017;2017. https://doi.org/10.1109/NAPS.2017.8107394.

[16] Rovatsos G, Jiang X, Dominguez-Garcia AD, Veeravalli VV. Comparison of statistical algorithms for power system line outage detection. In: 2016 IEEE international conference on acoustics, speech and signal processing (ICASSP), Mar. 2016, pp. 2946–2950, doi: 10.1109/ICASSP.2016.7472217.

[17] Emami R, Abur A. Tracking changes in the external network model. North Am. Power Symp. 2010, NAPS 2010, 2010, doi: 10.1109/NAPS.2010.5618980.

[18] Ahmed A, Awais M, Naeem M, Iqbal M, Alpalagan A. Efficient multiple lines outage detection in SmartGrid. 2015 Power Gener Syst Renew Energy Technol PGSRET 2015;2015. https://doi.org/10.1109/PGSRET.2015.7312243.

[19] Ahmed A, et al. Multiple power line outage detection in smart grids: probabilistic Bayesian approach. IEEE Access 2018;6:10650–61. https://doi.org/10.1109/ACCESS.2017.2710285.

[20] Tirtashi MRS, Svensson J, Samuelsson O. VSC-HVDC application to improve the long-term voltage stability. 2017 IEEE Manchester PowerTech Powertech 2017; 2017. https://doi.org/10.1109/PTC.2017.7980887.

[21] Polster S, Renner H, Samuelsson O, Friedl K. Advanced automated emergency control strategy for embedded VSC-HVDC links. e i Elektrotechnik und Informationstechnik forthcomming 2020;8:no. https://doi.org/10.1007/s00502-020-00831-8.

[22] Stott B, Jardim J, Alsaç O. DC power flow revisited. IEEE Trans Power Syst 2009;24 (3):1290–300. https://doi.org/10.1109/TPWRS.2009.2021235.

[23] Wood A, Wollenberg B, Sheble G. Power Generation, Operation, and Control. 3rd Editio. 2013.

[24] Kennedy J, Eberhart R. Particle swarm optimization. In: Proceedings of ICNN'95 - international conference on neural networks, 2016, vol. 4, no. 2, pp. 1942–1948, doi: 10.1109/ICNN.1995.488968.

[25] Polyak BT. Newton's method and its use in optimization. Eur J Oper Res 2007;181 (3):1086–96. https://doi.org/10.1016/j.ejor.2005.06.076.

[26] Bratton D, Kennedy J. Defining a standard for particle swarm optimization. Proc. 2007 IEEE Swarm Intell. Symp. SIS 2007, no. Sis, pp. 120–127, 2007, doi: 10.1109/SIS.2007.368035.

[27] Zambrano-Bigiarini M, Clerc M, Rojas R. Standard particle swarm optimisation 2011 at CEC-2013: A baseline for future PSO improvements. 2013 IEEE Congr Evol Comput CEC 2013;2013:2337–44. https://doi.org/10.1109/CEC.2013.6557848.

[28] Ghasemi M, Akbari E, Rahimnejad A, Razavi SE, Ghavidel S, Li L. Phasor particle swarm optimization: a simple and efficient variant of PSO. Soft Comput 2019;23 (19):9701–18. https://doi.org/10.1007/s00500-018-3536-8.

[29] Levenberg K. A method for the solution of certain non-linear problems in least squares. Q. Appl. Math., vol. 2, no. 2, pp. 164–168, 1944, [Online]. Available: https://www.jstor.org/stable/43633451.

[30] Marquardt Donald W. An algorithm for least-squares estimation of nonlinear parameters. J Soc Ind Appl Math, vol. 11, no. 2, pp. 431–441, 1963, [Online]. Available: https://www.jstor.org/stable/2098941.

[31] Ospina LDP, Correa AF, Lammert G. "Implementation and validation of the Nordic test system in DIgSILENT PowerFactory. 2017 IEEE Manchester PowerTech Powertech 2017;2017. https://doi.org/10.1109/PTC.2017.7980933.

[32] Report T. IEEE PES task force on test systems for voltage stability analysis and security assessment. Ieee, 2015, [Online]. Available: http://sites.ieee.org/pes-resource-center/files/2015/08/PES_TR19_Test-Systems-for-Voltage-Stability-Analysis-and-Security-Assessment1.pdf.

[33] "https://www.svk.se/en/grid-development/grid-projects/the-south-west-link/.".

[34] DigSilent. PowerFactory 2019, SP2 - Academic License. PowerFactory 2019, SP2 - Academic License, 2019. http://www.digsilent.de/.

[35] MathWorks. "https://de.mathworks.com/help/stats/fitdist.html.".